Measurement of the energy and multiplicity distributions of neutrons from the photofission of ^{235}U

S. D. Clarke,[1] B. M. Wieger,[1] A. Enqvist,[2] R. Vogt,[3,4] J. Randrup,[5] R. C. Haight,[6] H. Y. Lee,[6]
B. A. Perdue,[6] E. Kwan,[7] C. Y. Wu,[3] R. A. Henderson,[3] and S. A. Pozzi[1]

[1]*Department of Nuclear Engineering and Radiological Sciences, University of Michigan, Ann Arbor, Michigan 48109, USA*
[2]*Materials Science and Engineering, University of Florida, Gainesville, Florida 32661, USA*
[3]*Nuclear and Chemical Sciences Division, Lawrence Livermore National Laboratory, Livermore, California 94550, USA*
[4]*Department of Physics, University of California at Davis, Davis, California 95616, USA*
[5]*Nuclear Science Division, Lawrence Berkeley National Laboratory, Berkeley, California 94720, USA*
[6]*Los Alamos National Laboratory, Los Alamos, New Mexico 87545, USA*
[7]*National Superconducting Cyclotron Laboratory, Michigan State University, East Lansing, Michigan 48824, USA*

(Received 8 February 2017; published 20 June 2017)

For the first time, the complete neutron multiplicity distribution has been measured from the photofission of ^{235}U induced by high-energy spallation γ rays arriving ahead of the neutron beam at the Los Alamos Neutron Science Center. The resulting average neutron multiplicity 3.80 ± 0.08 (stat.) neutrons per photofission is in general agreement with previous measurements. In addition, unique measurements of the prompt fission energy spectrum of the neutrons from photofission and the angular correlation of two-neutron energies emitted in photofission also were made. The results are compared to calculations with the complete event fission model FREYA.

DOI: 10.1103/PhysRevC.95.064612

I. INTRODUCTION

Although there have been many measurements of neutron observables in the reaction ^{235}U(n,f), especially at thermal energies, similar measurements of neutron observables from photofission, ^{235}U(γ,f), are confined to energies near the threshold [1,2] and to measurements of average quantities only [3]. The latter are the only measurements of neutron observables that cover the giant dipole resonance in photonuclear fission of ^{235}U. Libraries of evaluated data, such as ENDF/B-VII must rely almost exclusively on models of photon-induced fission [4–7] to populate their databases. Data taken with a tunable monoenergetic photon source, such as the High Intensity γ-ray Source at Duke University in the United States where photon energies of up to 100 MeV are available, could also help replace models with experimental data [1,2].

We have measured several neutron observables from photofission on ^{235}U using a white photon source created by the high-energy γ rays arriving ahead of the neutron beam at the Los Alamos Neutron Science Center (LANSCE). Although the experiment was fielded to study neutron-induced fission on ^{235}U, the time-of-flight separation between the arrival of the spallation photons and the neutrons on the ^{235}U target made it possible, for the first time, to measure the neutron multiplicity distribution, prompt fission neutron spectrum, and two-neutron energy angular correlation from photofission.

In this paper, we describe the experimental setup and then compare the measured results to the complete-event fission model FREYA [8–12]. The experimental conditions are explained in Sec. II. Section III introduces FREYA, describes how it models photofission, and compares the data to FREYA calculations.

II. EXPERIMENTAL SETUP

This experiment was performed at the WNR-15L beam line at LANSCE where an 800-MeV pulsed proton beam impacts a tungsten target to produce neutrons and photons by spallation [13]. Neutrons and photons exiting the target at 15° from the incident proton beam are collimated and travel down a 21.502-m path into a parallel-plate avalanche chamber (PPAC) that contains approximately 112 mg of 99.91% ^{235}U deposited on both sides of ten plates [14]. The diameter of each ^{235}U deposit is 4 cm, resulting in an area of approximately 12.6 cm^2 on each plate. The plates are separated by approximately 1 cm. Each plate chamber can independently trigger, providing knowledge of the exact plate where each fission event occurs.

A. Experimental configuration

An array of 16 organic liquid scintillation detectors (EJ-309) was used in this experiment. Each detector was 7.62 cm in diameter and 5.08-cm thick. The detectors were placed approximately 22 cm away from the center of the fission chamber, arranged on two rings, each holding eight detectors with a total azimuthal angular coverage of approximately 270°. There is an angular separation of approximately 31° between detectors within a single arc. The center-to-center angle for neighboring detectors on opposite rings is approximately 45 polar angle degrees. A detection threshold of 40 keVee (approximately 0.5 MeV of deposited proton-recoil energy) was applied. Each detector was recalibrated several times during the experiment with a ^{137}Cs source to verify the stability of the high-voltage power supply and the consistency of the detector responses. A steel holder held in place by bands of aluminum supported the array. Figure 1 shows a photograph of the experimental setup. The experiment took place over a period of 2.5 weeks. Approximately 210 000 photofissions were recorded in the PPAC.

B. Data-acquisition system

The data were acquired using multiple time-synchronized CAEN V1720 digitizers that sampled the measured pulses at

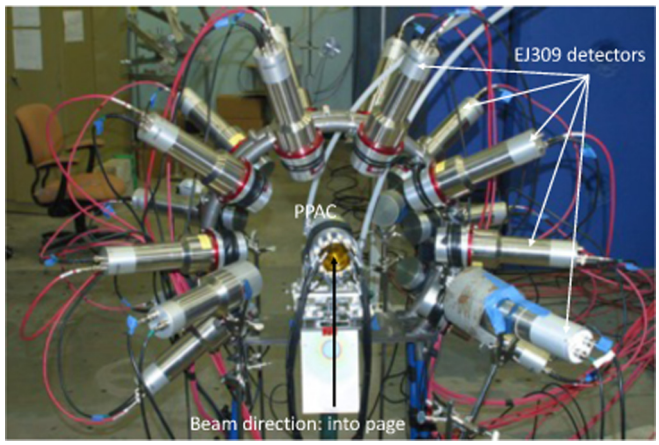

FIG. 1. Experimental setup used in 2012 measurement at LANSCE.

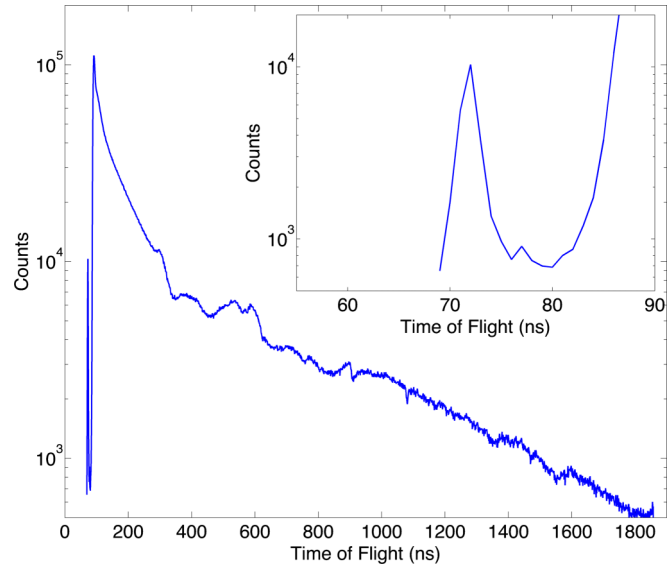

FIG. 2. The time distribution of fission triggers in the PPAC. The start time is defined as the time when the neutrons and γ rays are produced in the spallation target. The inset shows the fission events induced by photons at early times.

12 bits and 250 MHz. The digitized pulse data were stored for offline pulse shape discrimination (PSD) and time-correlation analyses. The custom software used for data acquisition was developed at the University of Michigan [15]. Four boards were synchronized to acquire events from different boards in the same time window, allowing each detector to be paired with individual PPAC plates. A combined trigger signal from all PPAC plates was sent to the digitizer boards to synchronize them. Signals from the beam, the detectors, and the individual plate channels were all sent to the digitizer. An event was recorded every time the PPAC triggered.

C. Data analysis

A variety of offline analysis techniques was applied to the acquired data: (i) rejecting unusable wave forms (such as clipped or piled-up pulses), (ii) finding and aligning the timing information of the collected pulses, and (iii) determining the particle type that created the wave form.

The PSD algorithms used for this experiment have been described in previous publications [16,17]. Prior to performing the PSD, pulses that satisfy one of the following criteria are rejected: (i) more than one pulse in the same detector time window, (ii) pulses that appear too early in the time window for proper timing, (iii) pulses that appear too early or too late in the pulse window to perform the full PSD integration, (iv) pulses that have negative tail integrals, and (v) pulses that appear clipped due to exceeding the digitizer dynamic range. After removing these pulses, individual pulse information is determined: timing, discrimination between neutron and photon events, pulse height, etc. From this output, a time-of-flight distribution is obtained by subtracting the detection time in the detector from the time of fission in the fission chamber. The pulse height distributions are constructed as a histogram of the maximum amplitudes of all detected pulses.

Background subtraction is performed using the time-of-flight distribution: the mean of a time slice before and after the region of interest is calculated. From this distribution, the slope of a line that represents the time-dependent background is calculated and then subtracted from the data.

Figure 2 shows the time distribution of PPAC fission triggers. When converted to energy, features in this distribution correspond to features in the ^{235}U neutron-induced fission cross section. Additional features correspond to the lead and polyethylene beam-line inserts. The inset of the plot shows the photofission peak with a FWHM of approximately 2.5 ns. These events are induced by the high-energy photons produced during the LANSCE spallation reaction that arrives at the fission chamber well separated in time from the fast neutrons.

III. RESULTS

In this section, the experimental results on the prompt fission neutron spectrum, neutron multiplicity distribution, and two-neutron-energy angular correlations from photofission are presented and compared to calculations using the complete-event fission model FREYA [8–12]. FREYA uses a combination of data and modeling for the required input distributions as a function of neutron energies for neutron-induced fission: the fission fragment mass yields $Y(A)$, assuming binary fission, and the total kinetic energy (TKE) of the two fragments as a function of heavy fragment mass TKE(A_H). Once the fragment masses and kinetic energies are chosen, the fragments are hot and rotating. They shed their rotational and excitation energy by emitting neutrons and then photons until the resulting product nucleus is in its ground state.

FREYA already was adapted to photofission for the calculation of the prompt neutron polarization asymmetries to compare with the data in Ref. [2]. In that case, the required yields for ^{238}U and ^{240}Pu were adapted from spontaneous fission data because no corresponding photofission yields were known to be available at the time. See Ref. [18] for some

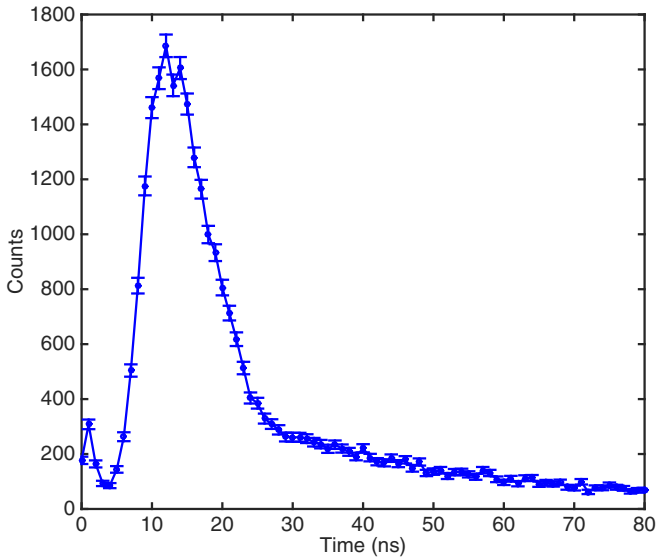

FIG. 3. Total neutron time-of-flight (from the fission chamber to each of the detectors) spectrum of neutrons emitted following photofission. The error bars are statistical uncertainties.

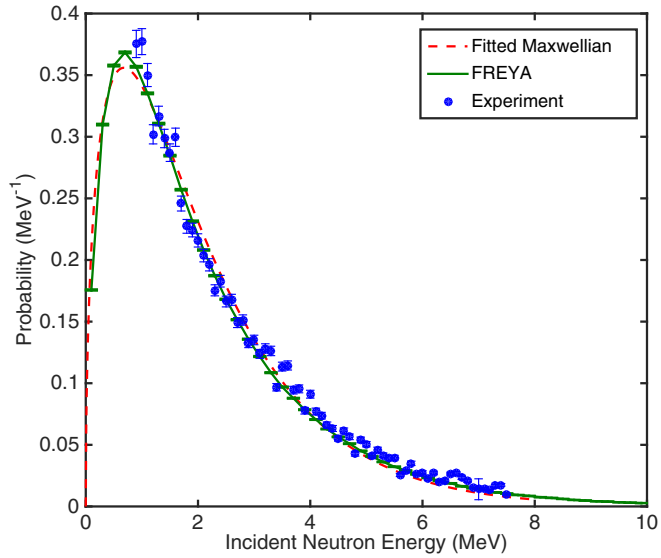

FIG. 4. The unit-normalized prompt fission neutron spectrum from ^{235}U(γ, f) incident on each of the detectors. The measured values are in blue. The red (dashed) curve is a Maxwellian spectrum fitted with $T_m = 1.38 \pm 0.04$ MeV, whereas the green (solid) curve is the FREYA calculation. The experimental error bars are statistical uncertainties.

appropriate benchmark data for ^{238}U(γ, f) and ^{234}U(γ, f); however, no such data for the yields and total kinetic energy are known for ^{235}U(γ, f). In this case, the neutron-induced fission yields are adapted by reducing the mass number appropriately starting from the ^{235}U(n, f) data and using the energy dependence of the neutron-induced fission yields for that compound nucleus in FREYA; none of the input parameters for FREYA were adapted from those of neutron-induced fission on ^{235}U.

Because the photon source is white, the energy of each photon-induced fission was unknown. To generate results in FREYA, the photofission component of the ^{235}U photonuclear cross section was used to sample the photon energy input for FREYA. The photofission cross section has a peak around 14 MeV, near the giant dipole resonance [19]. This peak is enhanced by the proximity of the second-chance photofission threshold around 12 MeV. The FREYA calculations allow for multichance fission in addition to first chance fission. In the calculations performed here, 62% of the total fissions were ^{235}U(γ, f), 38% were ^{235}U(γ, nf), and higher-order contributions were negligibly small. The results shown here for FREYA are a composite 10^6 events with incident photon energies averaged over the photofission cross section, assuming that the incident photon energy spectrum is flat over the giant dipole resonance (between approximately 10 and 20 MeV).

A. Neutron energy spectra

The energy distribution of prompt fission neutrons arriving at the detectors is calculated by first measuring the neutron time-of-flight distribution from the fissions induced by photons. The background is subtracted from the time-of-flight distribution, and the remaining flux is converted from time of flight into neutron energy using the known distances from the fission chamber to the detectors. Figure 3 shows the neutron time-of-flight distribution. The distribution in the range from 5 to 20 ns was divided into time bins corresponding to specific neutron energies as determined by the neutron flight path and arrival time. This time interval corresponds to neutrons with energies between 0.65 MeV (20 ns) and 10 MeV (5 ns). The resulting energy distribution was divided by the detector efficiency to obtain the number of neutrons in each energy bin. The detector efficiency was measured at the University of Michigan using a ^{252}Cf source placed 1.5 m from the detectors and a polyethylene shadow bar to reduce room return. Because the detected counts are fission-chamber triggered, the experimental background is minimal. However, the detectors have low efficiency for both low- and high-energy neutrons which could impact the shape of the measured neutron energy spectrum and the resulting fit.

The resulting prompt-fission neutron energy spectrum is fitted with a Maxwellian distribution,

$$N_m(E) = \sqrt{\frac{4}{\pi T_m^3}\sqrt{E}\exp\left(-\frac{E}{T_m}\right)}. \quad (1)$$

Figure 4 shows the resulting distribution, normalized to unity. The measured spectrum is truncated at 1 MeV because the simulated detector efficiency is understood poorly below this energy. Furthermore, the scattered neutron background becomes non-negligible at the longer times associated with these lower energies. The Maxwellian parameter T_m, determined from the data $T_m = 1.38 \pm 0.04$ MeV, is sometimes referred to as the Maxwellian temperature; the error is the 95% confidence interval determined by the curve-fitting software. The fitted value agrees well with the value of 1.41 MeV obtained from fitting the calculated FREYA spectrum with a Maxwellian; see Ref. [9] for a discussion of the fragment temperature

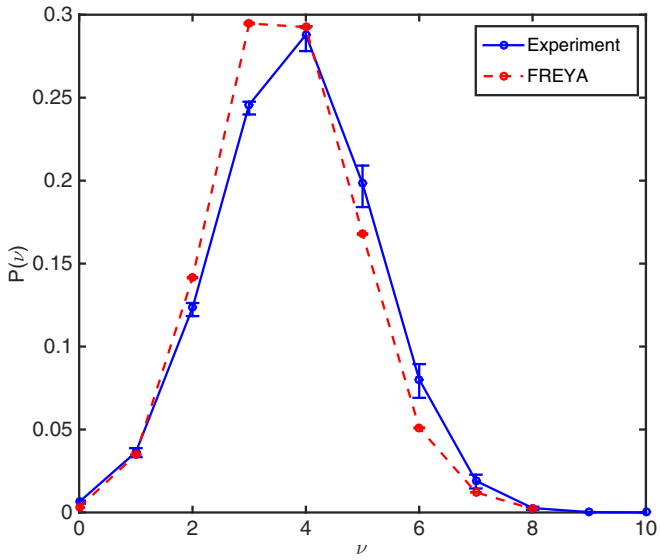

FIG. 5. The measured neutron multiplicity distribution from photofission with an experimental average of $\bar{\nu} = 3.80 \pm 0.08$ (stat.) (blue, solid curve); the FREYA simulation is shown by the red (dashed) curve. The error bars are statistical uncertainties.

in FREYA. An approximation of the prompt fission neutron spectrum by a Maxwellian with a single temperature parameter is convenient but cannot account for neutron emission from a cooling fragment as does a complete event model, such as FREYA. The ENDF/B-VII photonuclear library gives a value of 1.49 MeV [7], based on the original evaluation by Blokhin *et al.* [20]. This evaluation, described in Ref. [19], was based on data collected from 1955 to 1982 with white photon sources. The agreement of our results is within 7% of the ENDF/B-VII value, which is reasonable considering the sources of error in the experiment. Previous efforts to validate photonuclear data agreed within 10%–30% [5].

B. Neutron multiplicity distribution

Figure 5 shows the measured photofission neutron multiplicity distribution. The experimental $\bar{\nu}$ is found by counting the neutrons incident on the detectors and dividing by the number of fissions counted ∼210 000 in this experiment. To find the neutron multiplicity distributions, the detected neutron multiplicity distribution must be related to the actual number of neutrons emitted by the source. The following formula, originally derived for measurements employing a 4π detector [21], is used here:

$$P_\nu = \sum_{n=\nu}^{N} \frac{n!}{\nu!(n-\nu)!} \left(1 - \frac{1}{\varepsilon}\right)^{n-\nu} \left(\frac{1}{\varepsilon}\right)^{\nu} C_n. \qquad (2)$$

This relation gives the probability of emitting ν neutrons P_ν, based on the probability of observing C_n multiples of order n and the detection efficiency of the system ε. The scintillation detectors used in this experiment have an efficiency of 27.9% for an energy-averaged Watt spectrum and a 40-keVee detection threshold. Because the total solid angle subtended by the detectors is 1.24 sr, there is a 2.76% chance of detecting a single emitted neutron.

The average neutron multiplicity distribution $\bar{\nu}$ is calculated from

$$\bar{\nu} = \sum_{\nu=0}^{\infty} \nu P_\nu. \qquad (3)$$

The resulting average neutron multiplicity over the white photon source is 3.80 ± 0.08 where the error is solely determined from Poisson counting statistics. This value corresponds to photofission by approximately 16-MeV photons, according to the energy-dependent average values published by Caldwell *et al.* [3]. This energy is reasonable given the shape of the giant dipole resonance cross section, which peaks near 14 MeV. In comparison, FREYA predicts an average value of 3.62, about 2σ away from the measured value. In the FREYA simulation, the photon energy spectrum is assumed constant so that the events are weighted only by the evaluated photonuclear cross section. If the photon energy spectrum was not constant, a difference between the measured and the calculated values of $\bar{\nu}$ could be introduced. In addition, the data could be affected by detector cross talk and other accidental coincidences, which would slightly bias the data towards higher multiples. However, cross talk is most pronounced at low detector-pair angles, and, as seen in Fig. 6, the effect on the neutron energy correlation appears to be small.

C. Neutron energy-angle distribution

Figure 6 shows the average detected energy of a pair of correlated neutrons from photofission as a function of the angle between the detectors (blue points). The measured energies were obtained from the neutron time-of-flight energy distribution in correlated neutron events. More specifically, the reported energies are the average of the neutron time-to-energy conversion of all neutrons in a correlated event in detectors

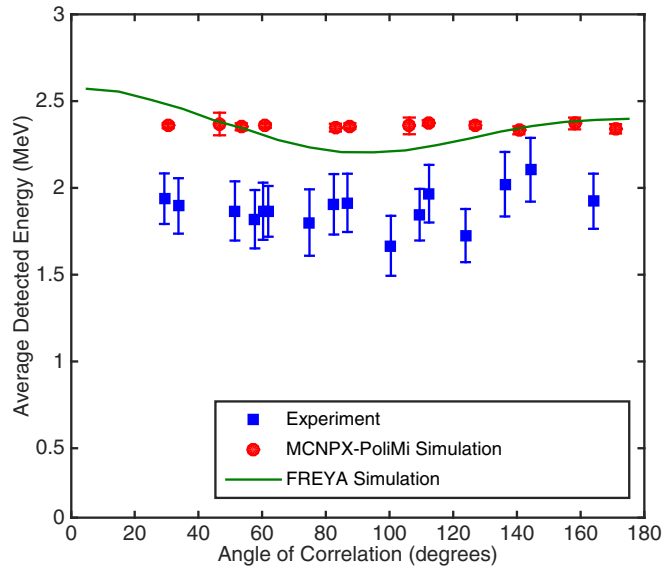

FIG. 6. Average detected energy of correlated photofission neutron pairs as a function of the angle between detectors.

within a specific angular bin; the angles are defined between the center-to-center detector angular separation as seen from the fission chamber origin. The data are relatively independent of the opening angle. The average value of the two detected neutrons is 1.90 ± 0.19 MeV. The uncertainty is dominated by the relatively short fission chamber to the detector flight path. The average energy of the Maxwellian distribution in Fig. 4 is 1.5 times the Maxwellian temperature parameter or 2.12 MeV, which is slightly above our measured value. The detected correlations are from fissions emitting at least two neutrons; most events on average emit more than two neutrons. It is expected that, as the number of neutrons emitted from fission increases, the energy spectrum will soften due to conservation of energy, which could explain why our measured value is slightly less than the average of the uncorrelated neutron energy spectrum. Additionally, detector cross talk could reduce the average energy at small correlation angles. The measured correlation seems relatively independent of angle, suggesting that cross talk is not significant for this experiment.

FREYA predicts an angle-averaged energy of 2.21 MeV after incorporating the energy-dependent detection efficiency; the angle-dependent distribution is shown by the green curve in Fig. 6. We can expect that each subsequent neutron emission in a single fission event reduces the available energy for further neutron emission so that the second detected neutron has an average energy somewhat less than that of the first neutron. Because the average neutron multiplicity is also rather high, 3.62 for FREYA in Sec. III B, the two neutrons paired in the correlation may not be the first two neutrons emitted during fission. This also can change the calculated average relative to $1.5T_m$ because neutrons emitted later have lower energy on average.

The FREYA result is not angle independent but shows a small modulation with enhancements at 0° and 180°. This dependence is consistent with FREYA calculations of two-neutron number correlations for spontaneous and neutron-induced fission where the enhancements come from the relative boost of the fragments since the neutrons are boosted along the line of motion of the mother fragment. The modulation is reduced since the average neutron multiplicity is rather high, consistent with the larger average photon energy. In Ref. [9], the largest modulations for two-neutron number correlations relative to 90° was found for spontaneously fissioning isotopes with average neutron multiplicities close to two.

We also simulated the two-neutron energy-angle correlation using MCNPX-POLIMI, shown by the red points in Fig. 6. This simulation represents an idealized case because neutrons are emitted isotropically. Thus, the simulated neutron energy is independent of the angular separation of the neutrons. The mean two-neutron energy of the MCNPX-POLIMI simulation is 2.4 MeV, still higher than the FREYA result. This discrepancy between the models, as well as the poorer agreement of MCNPX-POLIMI with the data, makes sense given that MCNPX-POLIMI does not include any particle or energy correlations.

Our measurements agree reasonably well with the FREYA calculations. Given that the FREYA calculations were not tuned to photofission and that the inputs yields were adopted from those at the corresponding energy for neutron-induced fission, discrepancies between the measurement and the simulations are not unexpected. Additional sources of differences may be found on the experimental side. The detectors measure neutrons primarily on the azimuthal plane which could bias the measured results. However, such a bias effect is difficult to quantify.

IV. CONCLUSIONS

We measured neutron observables from photofission on ^{235}U for the first time at LANSCE using a specially designed PPAC containing 112 mg of 99.91% ^{235}U. An array of fast liquid scintillators was used to measure the energy and multiplicity distributions of prompt photofission neutrons. An average of 3.80 ± 0.08 (stat.) neutrons per photofission was obtained from the measured data. In addition, the prompt fission neutron-energy spectrum from photofission was reported for the first time as was the two-neutron-energy correlation with the opening angle between the neutrons. The data were compared to FREYA simulations, which were not previously tuned specifically to reproduce neutron multiplicities from photofission. Despite this fact, reasonable agreement of the calculations with the data was found.

ACKNOWLEDGMENTS

This work was partially funded under the Department of Energy, Nuclear Engineering University Program (NEUP) Award No. DE-AC07-05ID14517-00120867. This work benefited from the use of the LANSCE accelerator facility, which is supported by the U.S. Department of Energy and Los Alamos National Laboratory under Contract No. DE-AC52-06NA25396. This work also was performed, in part, under the auspices of the U.S. Department of Energy by Lawrence Livermore National Laboratory under Contract No. DE-AC52-07NA27344 (R.V.) and by Lawrence Berkeley National Laboratory under Contract No. DE-AC02-05CH11231 (J.R.).

[1] L. Csige, D. M. Filipescu, T. Glodariu, J. Gulyás, M. M. Günther, D. Habs, H. J. Karwowski, A. Krasznahorkay, G. C. Rich, M. Sin, L. Stroe, O. Tesileanu, and P. G. Thirolf, Exploring the multihumped fission barrier of ^{238}U via sub-barrier photofission, Phys. Rev. C **87**, 044321 (2013).

[2] J. M. Mueller, M. W. Ahmed, B. Davis, J. M. Hall, S. S. Henshaw, M. S. Johnson, H. J. Karwowski, D. Markoff, L. S. Myers, B. A. Perdue, S. Stave, J. R. Tompkins, M. J. Tuffley, and H. R. Weller, Measurement of prompt neutron polarization asymmetries in photofission of ^{235,238}U, ^{239}Pu, and ^{232}Th, Phys. Rev. C **85**, 014605 (2012).

[3] J. T. Caldwell, E. J. Dowdy, R. A. Alvarez, B. L. Berman, and P. Meyer, Experimental determination of photofission neutron multiplicities for ^{235}U, ^{236}U, ^{238}U, and ^{232}Th using monoenergetic photons, Nucl. Sci. Eng. **73**, 153 (1980).

[4] M. B. Chadwick, P. G. Young, R. E. MacFarlane, M. C. White, and R. C. Little, Photonuclear physics in radiation transport–I: Cross sections and spectra, Nucl. Sci. Eng. **144**, 157 (2003).

[5] M. C. White, R. C. Little, M. B. Chadwick, P. G. Young, and R. E. MacFarlane, Photonuclear physics in radiation transport–II: Implementation, Nucl. Sci. Eng. **144**, 174 (2003).

[6] M.-L. Giacri-Mauborgne, D. Ridikas, M. B. Chadwick, P. G. Young, and W. B. Wilson, Photonuclear physics in radiation transport–III: Actinide cross sections and spectra, Nucl. Sci. Eng. **153**, 33 (2006).

[7] M. B. Chadwick, P. Obložinský, M. Herman, N. M. Greene, R. D. McKnight, D. L. Smith *et al.*, ENDF/B-VII.0: Next generation evaluated nuclear data library for nuclear science and technology, Nucl. Data Sheets **107**, 2931 (2006).

[8] J. Randrup and R. Vogt, Calculation of fission observables through event-by-event simulation, Phys. Rev. C **80**, 024601 (2009).

[9] R. Vogt and J. Randrup, Event-by-event study of neutron observables in spontaneous and thermal fission, Phys. Rev. C **84**, 044621 (2011).

[10] R. Vogt and J. Randrup, Event-by-event study of photon observables in spontaneous and thermal fission, Phys. Rev. C **87**, 044602 (2013).

[11] J. Randrup and R. Vogt, Inclusion of angular momentum in FREYA, Phys. Rev. C **89**, 044601 (2014).

[12] R. Vogt and J. Randrup, Study of neutron angular correlations in spontaneous and neutron-induced fission, Phys. Rev. C **90**, 064623 (2014).

[13] LANSCE and the 15L flight path at WNR are described at http://wnr.lanl.gov/_assets/flight_paths/4FP15L-A.php.

[14] C. Y. Wu, R. A. Henderson, R. C. Haight, H. Y. Lee, T. N. Taddeucci, B. Bucher, A. Chyzh, M. Devlin, N. Fotiades, E. Kwan, J. M. O'Donnell, B. A. Perdue, and J. L. Ullmann, A multiple parallel-plate avalanche counter for fission-fragment detection, Nucl. Instrum. Methods Phys. Res., Sect. A **794**, 76 (2015).

[15] A. Poitrasson-Rivère, M. Flaska, M. C. Hamel, K. Ide, J. K. Polack, S. D. Clarke, and S. A. Pozzi, in *2012 IEEE Nuclear Science Symposium and Medical Imaging Conference Record (NSS/MIC), Anaheim, CA, 2012* (IEEE, Piscataway, NJ, 2012), CD-ROM, pp.1597–1599.

[16] K. A. A. Gamage, M. J. Joyce, and N. P. Hawkes, A comparison of four different digital algorithms for pulse-shape discrimination in fast scintillators, Nucl. Instrum. Methods Phys. Res., Sect. A **642**, 78 (2011).

[17] M. Flaska and S. A. Pozzi, Identification of shielded neutron sources with the liquid scintillator BC-501A using a digital pulse shape discrimination method, Nucl. Instrum. Methods Phys. Res., Sect. A **577**, 654 (2007).

[18] A. Göök *et al.*, Fragment characteristics from fission of ^{238}U and ^{234}U induced by 6.5 - 9.0 MeV bremsstrahlung, Nucl. Phys. A **851**, 1 (2011).

[19] International Atomic Energy Agency, *Handbook on Photonuclear Data for Applications Cross-Sections and Spectra* (IAEA-TECDOC-1178, IAEA, Vienna, 2000).

[20] A. I. Blokhin, N. N. Buleeva, N. Nasyrova, and O. Pakhomoya, Preparation and use of "BOFOD" evaluated photoneutron data library, Vopr. At. Nauki Tekh., Ser.: Yad. Konstanty **3**, 3 (1992).

[21] B. C. Diven, H. C. Martin, R. F. Taschek, and J. Terrell, Multiplicities of fission neutron, Phys. Rev. **101**, 1012 (1956).